NASA TECHNICAL MEMORANDUM

NASA TM X-2647

NASA TM X-2647

EXPERIMENTAL STUDY OF WALL BOUNDARY-LAYER GROWTH IN THE 10° HALF-ANGLE CONICAL NOZZLE OF A REFLECTED-SHOCK TUNNEL

by Gene P. Menees

Ames Research Center
Moffett Field, Calif. 94035

NATIONAL AERONAUTICS AND SPACE ADMINISTRATION • WASHINGTON, D. C. • SEPTEMBER 1972

1. Report No. NASA TM X-2647	2. Government Accession No.	3. Recipient's Catalog No.
4. Title and Subtitle EXPERIMENTAL STUDY OF WALL BOUNDARY–LAYER GROWTH IN THE 10° HALF–ANGLE CONICAL NOZZLE OF A REFLECTED–SHOCK TUNNEL		5. Report Date September 1972 6. Performing Organization Code
7. Author(s) Gene P. Menees		8. Performing Organization Report No. A-4509
9. Performing Organization Name and Address NASA-Ames Research Center Moffett Field, Calif., 94035		10. Work Unit No. 112-02-20-01-00-21 11. Contract or Grant No.
12. Sponsoring Agency Name and Address National Aeronautics and Space Administration Washington, D.C. 20546		13. Type of Report and Period Covered Technical Memorandum 14. Sponsoring Agency Code

15. Supplementary Notes

16. Abstract

Calibration studies of shock-tunnel nozzle flow were made in both N_2 and Ar for a reservoir temperature of 2000° K and reservoir pressures of 15, 85, and 130 atm. The results for both test gases showed that the boundary layer was turbulent and the growth nonlinear, with the thickness being greater in Ar than N_2 at comparable reservoir conditions. The boundary-layer thickness decreased with increasing reservoir pressure, but only small differences occurred between the two largest reservoir pressures. Good correlations of the boundary layer and displacement thicknesses were obtained for both N_2 and Ar in terms of Reynolds number based on a reference temperature.

17. Key Words (Suggested by Author(s)) Boundary layers Turbulence Nozzle flow Compressible flow Gas dynamics	18. Distribution Statement Unclassified – Unlimited		
19. Security Classif. (of this report) Unclassified	20. Security Classif. (of this page) Unclassified	21. No. of Pages 29	22. Price* $3.00

* For sale by the National Technical Information Service, Springfield, Virginia 22151

SYMBOLS

$\frac{A}{A_*}$	local geometric area ratio (ratio at a nozzle axial station to throat area)
p	static pressure at centerline or side wall at a nozzle axial station, atm
p_{t_1}	total pressure in nozzle reservoir, atm
p_{t_2}	pitot pressure, atm
$\dot{q}_s$	stagnation-point heat-transfer rate, W/cm^2
Re	Reynolds number based on a reference temperature $\left(\frac{\rho_r u_e x}{\mu_r}\right)$
r	local nozzle radius at an axial station, cm
T_t	stagnation temperature, °K
T_r	reference temperature used to evaluate Re ($T_r = 0.25\ T_t$, a cold wall approximation defined in ref. 6), °K
u	velocity, cm/sec
x	axial distance from nozzle throat, cm
y	distance from nozzle wall, cm
δ	boundary-layer thickness, cm
δ_*	boundary-layer displacement thickness $\left(\frac{\delta_*}{\delta} = 1 - \int_0^1 \frac{\rho u}{\rho_e u_e}\ d\left(\frac{y}{\delta}\right)\right)$, cm
ρ	density, g/cm^3
μ	viscosity, g/cm-sec

Subscripts

e	boundary-layer edge
r	based on reference temperature (T_r)

EXPERIMENTAL STUDY OF WALL BOUNDARY–LAYER GROWTH IN THE 10° HALF–ANGLE CONICAL NOZZLE OF A REFLECTED–SHOCK TUNNEL

Gene P. Menees

Ames Research Center

SUMMARY

An experimental study of wall boundary-layer growth in the 10° half-angle conical nozzle of a reflected-shock tunnel is described. Calibrations were made with N_2 and Ar for a reflected-shock reservoir temperature of approximately 2000° K and reservoir pressures of about 15, 85, and 130 atm. Radial surveys of pitot pressure and stagnation-point heat-transfer rate, and centerline and side-wall measurements of static pressure were obtained. For the reservoir pressure of 85 atm, radial profiles of velocity and density were deduced from the experimental measurements and used to determine the boundary-layer displacement thickness.

The results of the study for both test gases showed that the boundary layer was turbulent and the growth nonlinear, with the thickness being greater in Ar than N_2 for comparable reservoir conditions. The boundary-layer thickness decreased with increasing reservoir pressure, but only small differences occurred between reservoir pressures of 85 and 130 atm. Good correlations of δ/x and δ_*/x were obtained for both N_2 and Ar in terms of Reynolds number based on a reference temperature.

INTRODUCTION

This paper describes calibration studies to determine the effects of wall boundary layer on the flow characteristics of the 10° half-angle conical nozzle of a reflected-shock tunnel. The motivation for these studies was the use of the nozzle for extensive gasdynamic-laser and chemical kinetic studies using mixtures of CO in N_2 and Ar (ref. 1). Since a knowledge of the expanding flow environment is essential for the proper analysis of data taken in the nozzle, it was necessary to establish the extent and uniformity of the inviscid flow by determining the nozzle boundary-layer growth.

The nozzle boundary layer was investigated at several axial stations by making radial surveys of pitot pressure and stagnation-point heat-transfer rate, and centerline and side-wall measurements of static pressure. For some conditions, sufficient pitot-pressure and stagnation-point heat-transfer data were obtained to deduce local profiles of velocity and density relative to corresponding values on the nozzle centerline. These results were used to determine the boundary-layer displacement thickness growth along the nozzle. The static pressure is a more sensitive detector of inviscid stream conditions than either pitot pressure or stagnation-point heat transfer and, therefore, is a valuable adjunct in defining the thermogasdynamic environment of the nozzle flow.

Since the gasdynamic laser and chemical kinetic studies performed in the nozzle primarily used mixtures of $CO–N_2$ or $CO–N_2–Ar$ with small percentages of CO, the nozzle was calibrated with N_2 and Ar to minimize real gas effects. The calibration studies were made for reservoir pressures of approximately 15, 85, and 130 atm and a reservoir temperature of about 2000°K for both N_2 and Ar.

The present paper presents, primarily, the experimental results of the nozzle flow calibration tests. However, some analysis is included, and experimental results for nozzle wall boundary-layer growth and inviscid stream conditions are compared with appropriate prediction techniques.

EXPERIMENTAL APPARATUS AND INSTRUMENTATION

Shock-Tunnel Design and Operation

The test facility is a conventional shock-tube arrangement and is shown schematically in figure 1(a). Both the driver and driven tubes are 10.2 cm in diameter and 3.51 and 11.43 m long, respectively, For the present tests, He was used as the driver gas and could be charged up to pressures of 200 atm at ambient temperature. The driven tube was evacuated to a pressure of about 20 μHg and then filled with the test gas, either N_2 or Ar, at ambient temperature to pressures near 1 atm. The 10° half-angle conical nozzle was attached to the end of the driven tube and exhausted into a large dump tank. The nozzle and dump tank were isolated from the driven tube by a thin diaphragm of polyethylene tape and were evacuated to a pressure of about 5 μHg before flow. Flow is initiated in the system by venting the chamber between the double diaphragm arrangement separating the driver and driven tube. A slug of high-temperature, high-pressure test gas having a nearly steady-state duration of several milliseconds is obtained after reflection of the incident shock wave from the driven-tube end wall. This slug of test gas acts as the reservoir for the conical nozzle, which has a throat diameter of 1.27 cm and an exit diameter of 76 cm. The nozzle throat contours to the driven-tube end wall with a 0.635-cm radius. Downstream of the throat, the nozzle contours to the 10° cone through a 6.35-cm radius transition section. The throat contour is shown in figure 1(a).

Driven-Tube Instrumentation

The downstream portion of the driven tube was instrumented with Atlantic Research LD-25 piezoelectric pressure transducers, which act as time-of-arrival indicators for the incident shock wave. These transducers have a sensitivity of 2.21 V/atm and a rise time of 1 μsec. The transducers were spaced at 1.22-m intervals along the driven tube with the last instrument port located 6.1 cm from the end wall. The elapsed time for passage of the incident shock between the various measuring stations is obtained from electronic counters, which are stopped by the transducer output signals. The last station in the driven tube was also instrumented with a Kistler 601-H piezoelectric transducer to monitor reservoir pressure. This transducer has a pressure range to 1000 atm, a sensitivity of 14.7 picocoulomb/atm, and a rise time of 3 μsec.

Nozzle Instrumentation

The nozzle was instrumented for flow measurements at geometric area ratios of 128, 576, 1444, and 2704, as shown in figure 1(a). Radial surveys of pitot pressure and stagnation-point heat-transfer rate were obtained at the three downstream stations. Only centerline pitot pressure was measured at the station nearest the nozzle throat. Static pressure measurements were obtained on the nozzle side wall at all four instrument stations and on the centerline at the three downstream stations.

All pitot- and static-pressure measurements, except the pitot pressure at the station nearest the nozzle throat, were made with stretched-diaphragm, variable-capacitance type pressure cells developed at the Ames Research Center. These pressure cells have design characteristics that are particularly suitable for low-pressure measurements in shock tunnel applications, such as low acceleration and temperature sensitivities and a relatively high natural frequency (~20 kHz). These characteristics are obtained by choice of diaphragm material and the application of uniform tensile loading to the diaphragm during fabrication. For the present tests, cells with several pressure ranges were used to span the different test conditions. The cell diaphragms were constructed of invar and were 0.635 cm in diameter. The diaphragm thickness ranged from 0.004 to 0.013 cm, and the cell sensitivities varied from 0.29 to 29.4 picofarad/atm. Static calibrations of the pressure cells were obtained before and after each test run for the expected pressure range. The calibrations were linear and repeatable to within a few percent. The pitot pressure at the station nearest the nozzle throat was measured with a Kistler 701-A piezoelectric transducer, which has a range to about 2 atm. A typical pitot-pressure probe configuration is shown in figure 1(b).

Both side-wall and centerline static-pressure measurements were made in the present tests since boundary-layer thicknesses were expected to be large, with possibly some pressure variation through the boundary layer. For the side-wall measurements, it was necessary to isolate the pressure cell from shock loads transmitted through the nozzle from the driven tube. This was accomplished by mounting the cell in a heavy brass housing, which was prevented from contacting the nozzle wall by "O" rings. The stiffness of the mount could be controlled by mechanical compression. The natural frequency of the entire arrangement was much less than the "ring frequency" of the nozzle wall. The pressure cell diaphragm was recessed from the nozzle wall and protected by a perforated brass cover, which acted as a shield and heat sink to minimize temperature effects. The side-wall, static-pressure cell mount is shown in figure 1(c). The cavity between the pressure cell diaphragm and perforated brass cover was designed for minimum volume to achieve filling times of about 1 msec.

The centerline measurements of static pressure were obtained by means of the specially designed probe shown in figure 1(d). The probe consists of a 10° ogive cylinder having a nose-fineness ratio of 10.9. The static-pressure orifice was located 20 diameters from the probe tip. Surface heat-transfer-rate measurements were also obtained by means of a thin wall calorimeter located on the probe at about 8 diameters downstream from the static-pressure orifice. These data were used to correct the measured static pressure for low-density, hypersonic flow effects according to the method of reference 2. The correction did not amount to more than 10 percent for the present tests.

The stagnation-point heat-transfer-rate measurements were obtained with calorimeter gages consisting of number 40 chromel-constantan thermocouples mounted in copper hemispheres. Two thermocouples were positioned near the stagnation point of each hemisphere. The hemispheres were 2.54 cm in diameter and had a wall thickness of 0.013 cm. The heat-transfer-rate data were repeatable to about ±10 percent.

Data-Recording Apparatus

The high-frequency data obtained from the shock-tunnel tests were recorded photographically by multiple oscilloscopes and digitally by a high-speed recorder system designed for the test facility. The digital data acquisition system (ref. 3) provides the experimental data in a form convenient for computer analysis.

DISCUSSION OF RESULTS

The nozzle flow calibration studies were made with N_2 and Ar as the test gases. Data were obtained for reflected-shock reservoir pressures of approximately 15, 85, and 130 atm at a total reservoir temperature of about 2000° K. The nozzle wall boundary-layer growth was determined from radial surveys of pitot pressure and stagnation-point heat transfer and centerline and side-wall measurements of static pressure.

Calibration Results with N_2

The results for the N_2 calibration studies are given in figures 2 through 8. For the conditions of the present tests, the vibrational excitation of N_2, determined from a real-gas stream-tube computer program, was found to be small. It also was determined that the N_2 freezes within about 2 cm of the nozzle throat. For these circumstances, the effect of the vibrational relaxation of N_2 is negligible, and the N_2 behaves, essentially, as an ideal gas.

Temporal variations of pitot pressure in a typical radial survey are shown in figure 2. These results were obtained for a reservoir pressure of about 85 atm at a nozzle area ratio of 1444. The corresponding reservoir pressure variation is also shown in figure 2(a); the arrival of the incident and reflected shock waves are indicated by the small and large pressure steps, respectively. These reservoir conditions result from nearly tailored operation of the shock tube (shock Mach number $\sim$ 4). A computed reservoir pressure based on the measured shock wave speed is also shown in figure 2(a). Computed reservoir pressures typically agreed to within 5 to 10 percent of the pressure measured immediately behind the reflected shock wave. The pitot-pressure curves shown in figure 2 indicate good flow uniformity and radial symmetry about the nozzle centerline. After the pitot pressures reach plateaus, the response curves at all five radial positions shown vary in accordance with the reservoir pressure.

The experimental pitot-pressure measurements can indicate the duration and uniformity of the nozzle test flow, as well as the behavior of the starting process. Similarly, the reservoir pressure indicates the steady-state character of the slug of test gas processed by the reflected shock. The results of figure 2 indicate about 1.5 msec of nearly steady-state reservoir and nozzle flow conditions. The nozzle starting time is also observed to be about 0.8 msec at this axial location. A somewhat more definitive indication of flow duration can be obtained from the radiation intensity histories of the laser studies conducted with the nozzle, since the radiation data show both temperature and pressure influences. The laser experiments reported in reference 1 provide temporal variations of radiation intensity in the reflected-shock reservoir and at several axial locations in the nozzle for mixtures of

CO with N_2 or Ar. These data corroborate the flow duration times indicated here by pressure measurements.

A typical radial pitot pressure distribution corresponding to the flow conditions of figure 2 is presented in figure 3. The distribution is generally uniform across the inviscid core with a rapid reduction in pressure as the boundary layer is encountered. The flow exhibits good radial symmetry, as in figure 2. There is also a slight indication of the pressure peaking at a radial distance of about $y/r = \pm 0.7$ from the nozzle centerline. This effect could be attributed to the interaction between the inviscid hypersonic flow and the boundary layer as discussed by Agafonov in reference 4. The results of figure 3 are typical of the radial distributions of pitot pressure obtained in N_2 at other nozzle locations and test conditions.

A typical radial distribution of stagnation-point heat-transfer rate corresponding to the flow conditions of figures 2 and 3 is shown in figure 4. This distribution indicates about the same size for the inviscid core as the pitot-pressure distribution of figure 3. The pitot-pressure and stagnation-point heat-transfer results of figures 3 and 4 can be used to deduce profiles of velocity and density through the boundary layer. These results are integrated to obtain the boundary-layer displacement thickness as discussed in reference 5. Sufficient data for this computation were available only for the 85-atm reservoir pressure data and the results are presented subsequently.

The axial distribution of pitot pressure along the nozzle for the various experimental reservoir pressures is shown in figure 5. The predicted pressure distributions for the inviscid one-dimensional expansion of both a perfect gas and equilibrium N_2 are shown for comparison. The difference between the measured and calculated pressures is due to nozzle wall boundary-layer growth. The horizontal separation indicates the effect of the boundary layer on the nozzle area ratio. The boundary-layer displacement thickness along the nozzle (for $p_{t_1} = 85$ atm) was determined from the radial distributions of pitot pressure and stagnation-point heat transfer as discussed previously. The extent of the effective inviscid core was determined from the computed boundary-layer displacement thickness and the nozzle geometry. The pitot-pressure distribution resulting from this inviscid area ratio and perfect gas expansion is shown in figure 5 and is seen to agree well with the measurements.

The axial distributions of static pressure along the nozzle centerline and side wall are presented in figure 6 for the various experimental conditions. Good agreement was generally obtained between the measurements at the two locations. Predictions for inviscid perfect gas and equilibrium pressure distributions, and the results obtained by correcting the inviscid core for the computed boundary-layer displacement thickness are shown in figure 6 for comparison. The latter distribution was obtained for perfect-gas expansion and coincides closely with that obtained by determining the extent of the inviscid flow from the measured pitot pressures.

The results for the nozzle wall boundary-layer growth are presented in figure 7 for the range of experimental reservoir conditions. In determining δ, the boundary-layer edge was defined as the location in the flow where the pitot pressure decreased to 99 percent of its peak value. As mentioned previously, sufficient experimental data were available to compute δ_* from deduced profiles of velocity and density only for the reservoir pressure of 85 atm. However, for all three test reservoir pressures, an estimate of δ_* was obtained from the measured pitot pressures. The δ_* obtained in this manner was determined from the nozzle geometry and inviscid area ratio corresponding to the measured $(p_{t_2}/p_{t_1})_e$. The results for the reservoir pressure of 85 atm agreed closely with those computed from the deduced profiles of velocity and density. The measured values for δ and δ_* are compared with predicted values obtained from the empirical equations of reference 6 for turbulent

boundary-layer growth in conical nozzles. For the range of Reynolds numbers of the present investigation (3.5×10^5 to 2.5×10^6), the wall boundary layer was assumed to be turbulent with transition from laminar to turbulent flow occurring near the nozzle throat. This assumption was verified by comparing the measured values of δ and δ_* with results obtained by laminar and turbulent prediction techniques. Agreement with the laminar predictions was poor, whereas the turbulent predictions of reference 6 agree well with the measured values of δ and δ_* as can be observed in figure 7.

The results of figure 7 show that the boundary-layer growth is nonlinear, with a considerable decrease in boundary-layer thickness as the reservoir pressure is increased from 15 to 85 atm. However, there is little additional change in the boundary-layer thickness as the reservoir pressure is further increased to 130 atm. The nonlinear growth of the boundary layer indicates that the viscous flow effects induce some deviation from one dimensionality in the inviscid flow. However, the static pressure measurements of figure 6 indicate this effect is small for the N_2 calibration results.

A correlation of δ_*/x, independent of Mach number, in terms of Reynolds number based on a reference temperature is suggested in reference 6. The result of applying this correlation to the present experimental data is shown in figure 8, with the correlation equations. As shown, the present data correlate well. Results for δ/x were also correlated in terms of the reference Reynolds number and are presented in figure 8. Note that although there is no precedent for this correlation, the boundary-layer thickness does correlate well in this manner, also.

Calibration Results With Ar

The results for the calibration studies with Ar as the test gas are given in figures 9 through 13. The temporal variation of reservoir and pitot pressures is not shown, since the results are similar to those for the N_2 tests presented in figure 2. The radial distribution of pitot pressure in a typical survey is shown in figure 9 at a nozzle area ratio of 1444 and reservoir pressure of 85 atm. The distribution is generally uniform across the inviscid core and symmetric with respect to the nozzle centerline. There is no indication of radial peaking of the pitot-pressure distribution for the conditions of figure 9. However, for the reservoir pressure of 15 atm, there was noticeable peaking at the two downstream nozzle stations with area ratios of 1444 and 2704. As noted earlier, this may result from the interaction between the boundary layer and hypersonic inviscid flow as discussed in reference 4. The results of figure 9 also indicate that the boundary-layer thickness is greater in Ar than in N_2 at the corresponding condition (fig. 3). This is generally true and will be discussed in more detail subsequently. A radial distribution of stagnation-point heat-transfer rate is not shown, since the results are similar to those for N_2. The boundary-layer displacement thickness along the nozzle was obtained from the radial distributions of pitot pressure and stagnation-point heat-transfer rate for a reservoir pressure of 85 atm, as was done for N_2.

The axial pitot-pressure distributions along the nozzle centerline are shown in figure 10 for the various experimental conditions. The results for the three reservoir pressures are in fair agreement. The largest deviation occurs for the reservoir pressure of 15 atm at the two downstream stations in the nozzle where the boundary-layer thickness is greatest. The predicted axial pressure distribution for the one-dimensional expansion of a perfect gas is shown in figure 10 to illustrate the extent of the wall boundary-layer growth. For a reservoir pressure of 85 atm, the effective inviscid area ratio was determined from the nozzle geometry and computed values of δ_* as discussed previously. The predicted axial pressure distribution corresponding to the effective inviscid area ratio is shown in figure 10 and agrees closely with the experimental results.

The axial distributions of static pressure along the nozzle are shown in figure 11. Close agreement was generally obtained between the measurements on the nozzle centerline and side wall. The maximum differences amounted to about 15 percent and occurred at the downstream stations in the nozzle where the boundary-layer thickness was greatest. The predicted axial pressure distribution for the one-dimensional expansion of an inviscid perfect gas and the distribution obtained by determining the effective inviscid core from the computed δ_* are also given in figure 11. Good agreement is obtained between the predicted and measured results at the two upstream stations in the nozzle, but considerable deviation is observed at the two downstream stations. This large difference between the measured and predicted static pressures downstream in the nozzle is attributed to the large boundary-layer thickness, which is of the order of 50 percent of the local nozzle radius. The present results are not sufficiently quantitative to determine the influence of viscous-effects and non-one-dimensional behavior of the inviscid flow on the measured static pressures.

The axial development of the nozzle wall boundary layer is shown in figure 12 for the three experimental reservoir conditions. The boundary layer growth is nonlinear and the thickness is greater than that for N_2 at comparable reservoir conditions. As was the case for N_2, there is a considerable decrease in boundary-layer thickness as the reservoir pressure is increased from 15 to 85 atm but essentially no additional change as the reservoir pressure further increases to 130 atm. No empirical formulas were available for predicting the growth of δ and δ_* in conical nozzles for the Ar calibration results. However, the semiempirical method of reference 6 for obtaining the development of δ_* in equivalent flat-plate flow for a turbulent boundary layer was adapted to Ar. The results are shown in figure 12, which indicates good agreement with the measured results for δ_*.

The correlation of δ_*/x and δ/x in terms of the reference Reynolds number was applied to the Ar data; the results and correlation equations used are shown in figure 13. It is observed that good correlations are obtained for both δ_*/x and δ/x.

CONCLUDING REMARKS

The 10° half-angle conical nozzle of a reflected-shock tunnel has been calibrated to obtain the wall boundary-layer growth in N_2 and Ar for a reservoir temperature of 2000° K and reservoir pressures of 15, 85, and 130 atm. The results of the study for both test gases showed that the boundary layer was turbulent and the growth nonlinear, with the thickness being greater in Ar than N_2 for comparable reservoir conditions. The boundary-layer thickness decreased with increasing reservoir pressure but only small differences occurred between reservoir pressures of 85 and 130 atm. Good correlations of δ/x and δ_*/x in terms of Reynolds number based on a reference temperature were obtained for both N_2 and Ar.

Ames Reserach Center
National Aeronautics and Space Administration
Moffett Field, Calif. 94035, June 21, 1972

REFERENCES

1. McKenzie, Robert L.: Five-Micron Laser Radiation From a Carbon Monoxide Gasdynamic Expansion. NASA TM X-62, 006, 1970.

2. Guy, R. W.; and Winebarger, R. M.: Effect of Orifice Size and Heat-Transfer Rate on Measured Static Pressures in a Low-Density Arc-Heated Wind Tunnel. NASA TN D-3829, 1967.

3. Seegmiller, H. Lee; and Mazer, Louis: A 500,000 Sample Per Second Digital Recorder for the Ames Electric Arc Shock Tunnel. ICIASF 1969 Record, pp. 243-247.

4. Agafonov, V. P.: Interaction Between the Boundary Layer and the Hypersonic Flow in a Conical Nozzle. Rep. ATD-66-54, May 16, 1966, Aerospace Technology Division, Library of Congress Translation.

5. Dunn, Michael G.: Experimental Study of High-Enthalpy Shock-Tunnel Flow. Part II: Nozzle-Flow Characteristics. AIAA J., vol. 7, no. 9, Sept. 1969. pp. 1717-1736.

6. Burke, A. F.: Turbulent Boundary Layers on Highly Cooled Surfaces At High Mach Numbers. CAL Rep. 118, 1961.

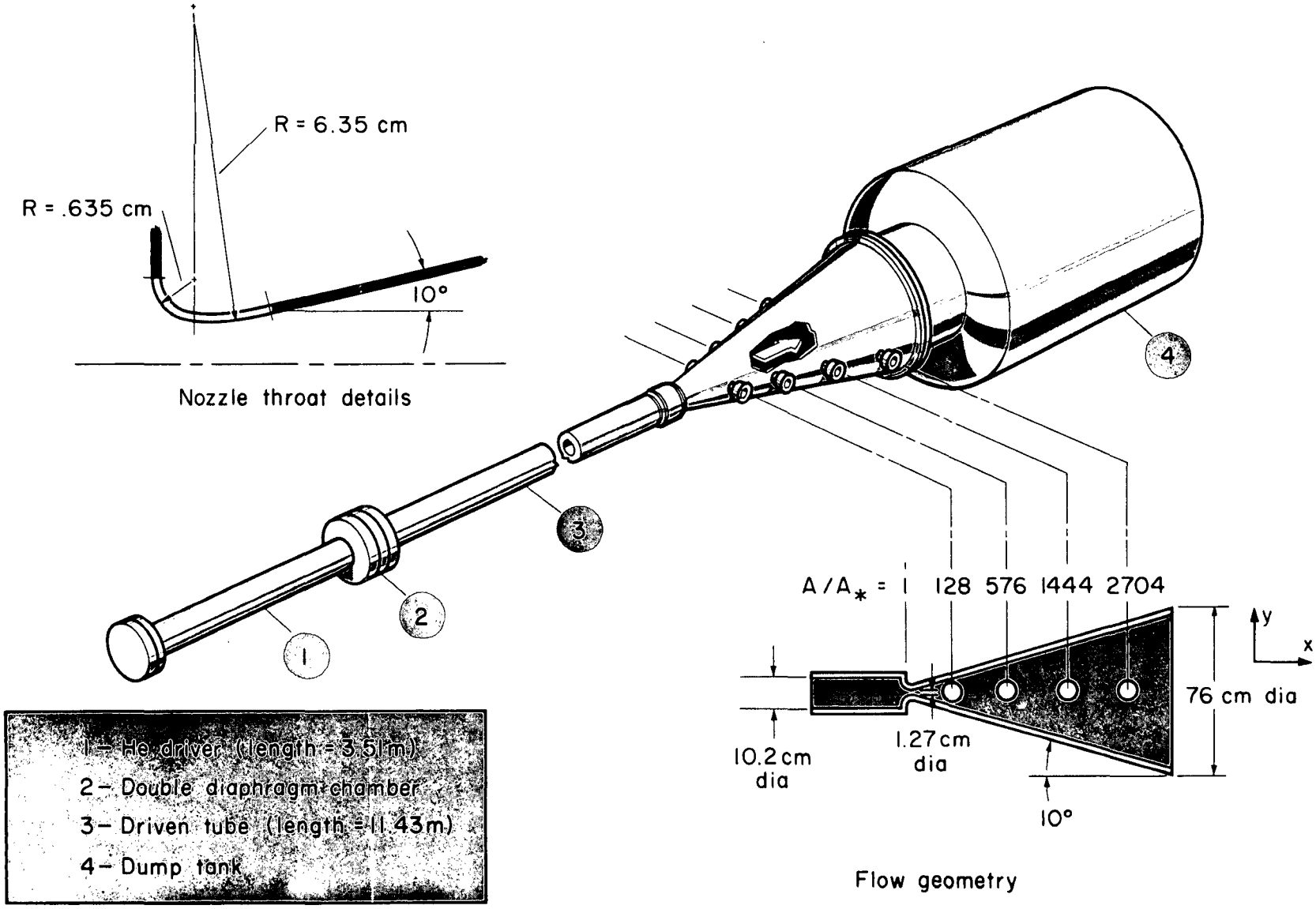

(a) Test facility.

Figure 1.– Details of test facility and instrumentation.

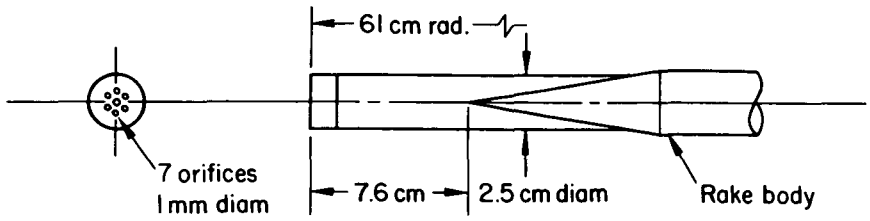

(b) Pitot pressure probe.

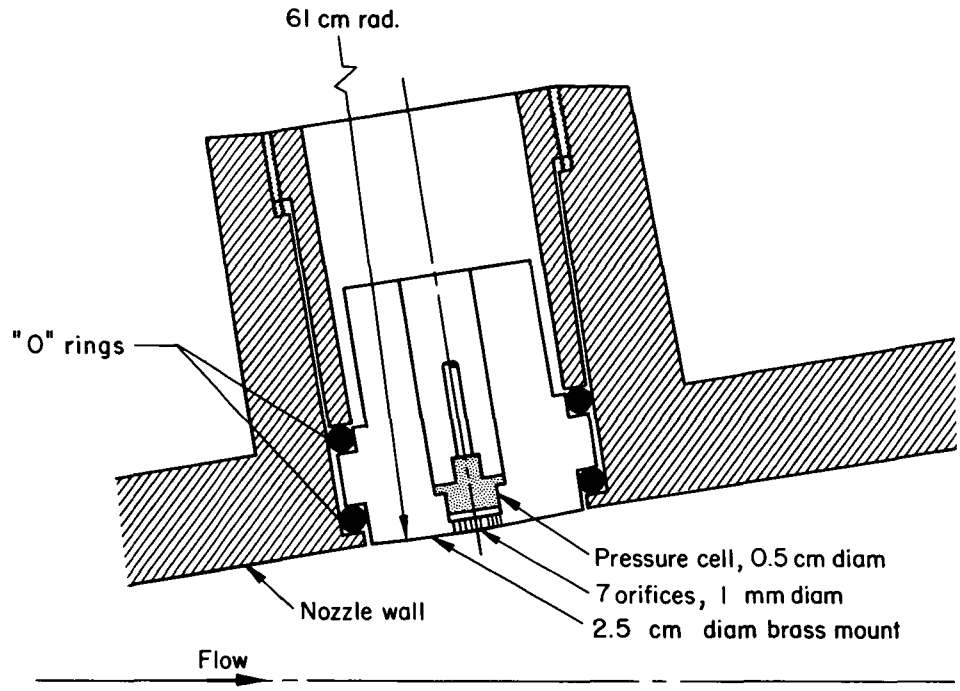

(c) Side-wall static-pressure cell mount.

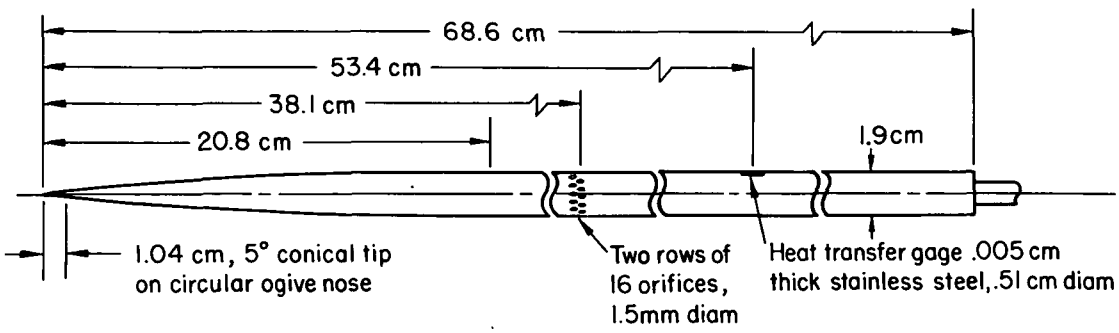

(d) Centerline static pressure probe.

Figure 1.– Concluded.

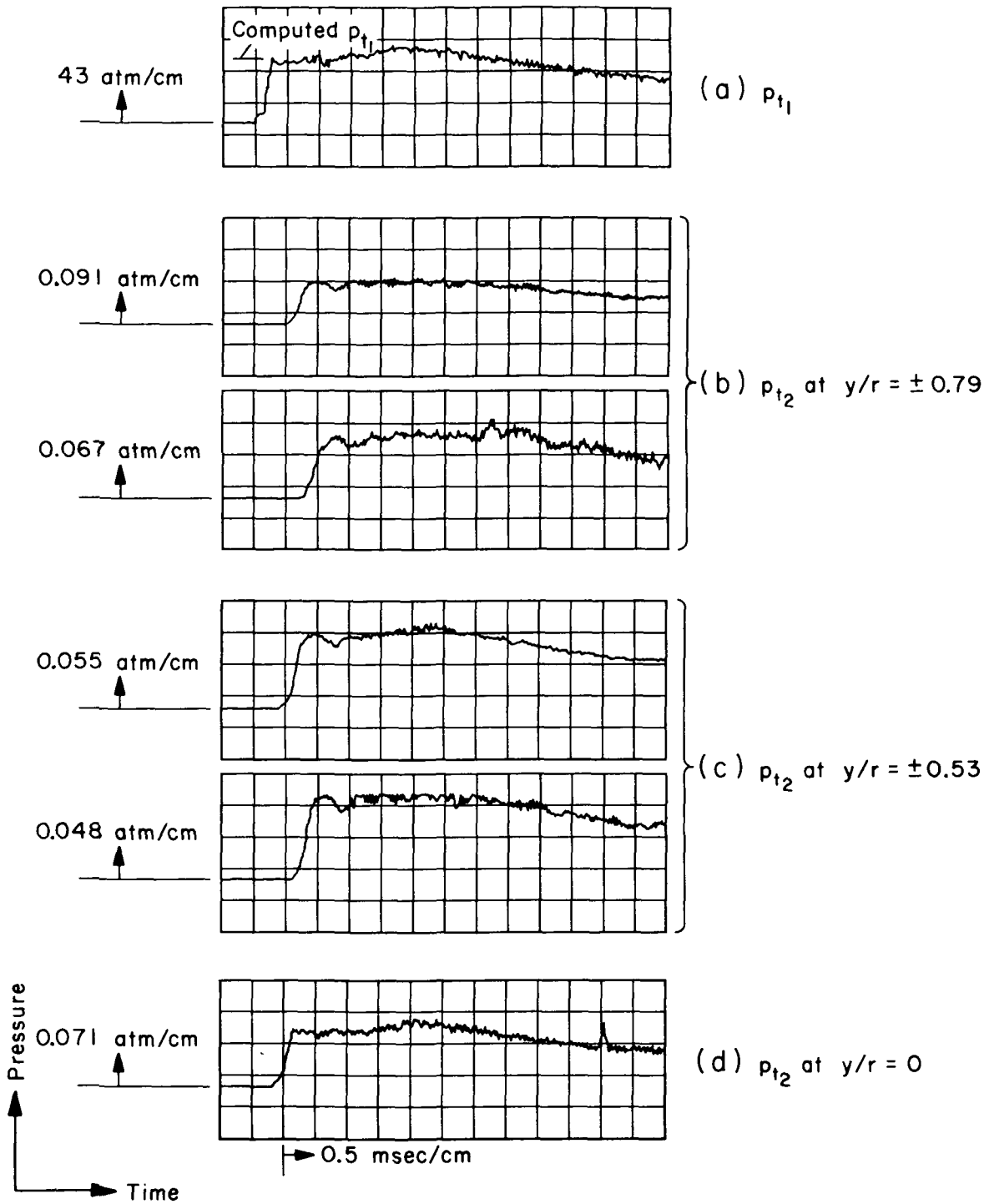

Figure 2.– Typical reservoir- and pitot-pressure response curves for a radial survey at $A/A_* = 1444$ with N_2 as the test gas; p_{t_1} ~85 atm.

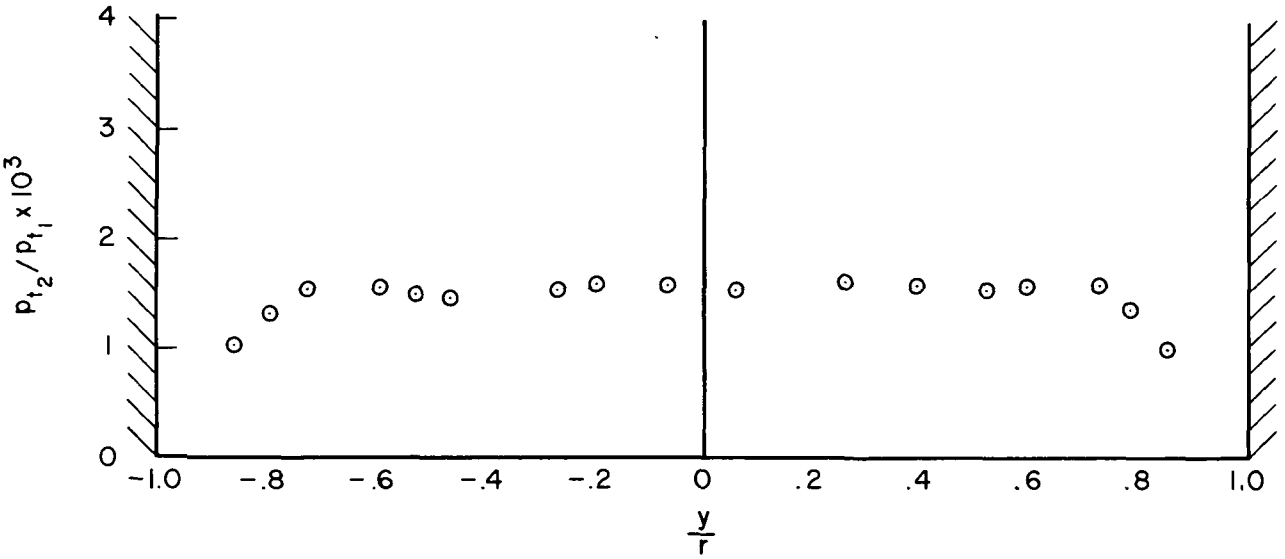

Figure 3.– Radial distribution of pitot pressure in N_2 at $A/A_* = 1444$; $p_{t_1} \sim 85$ atm, $T_t \sim 2000°$ K.

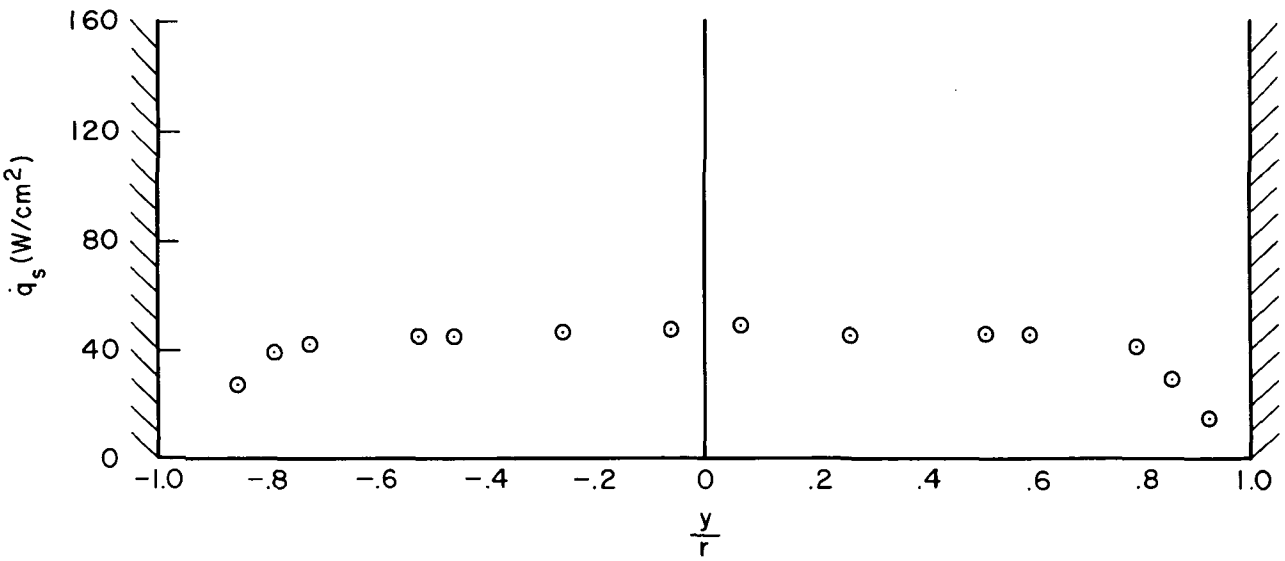

Figure 4.– Radial distribution of stagnation-point heat-transfer rate in N_2 at $A/A_* = 1444$; $p_{t_1} \sim 85$ atm , $T_t \sim 2000°$ K.

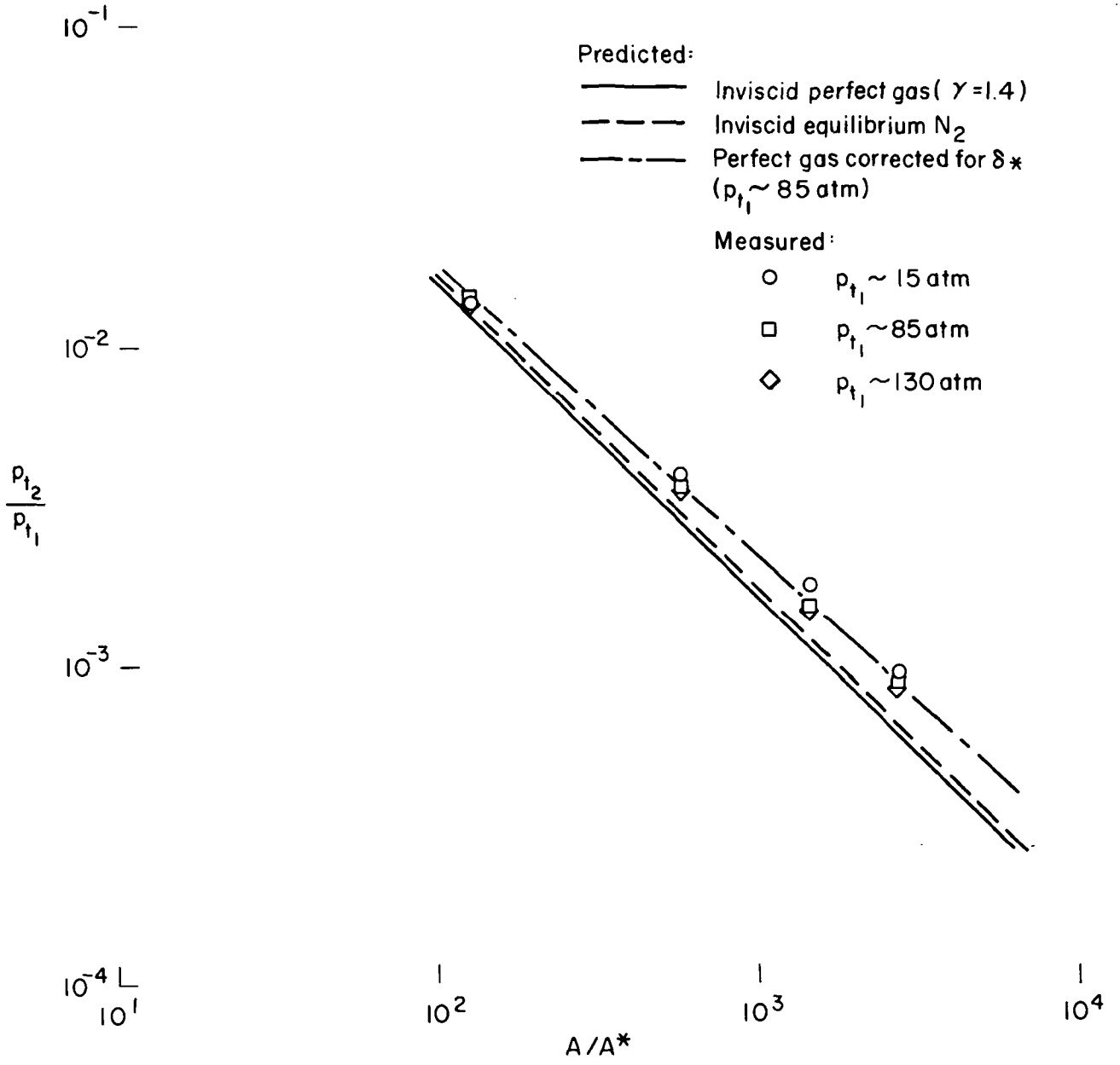

Figure 5.– Comparison of measured and predicted axial pitot-pressure distributions in nozzle for N_2.

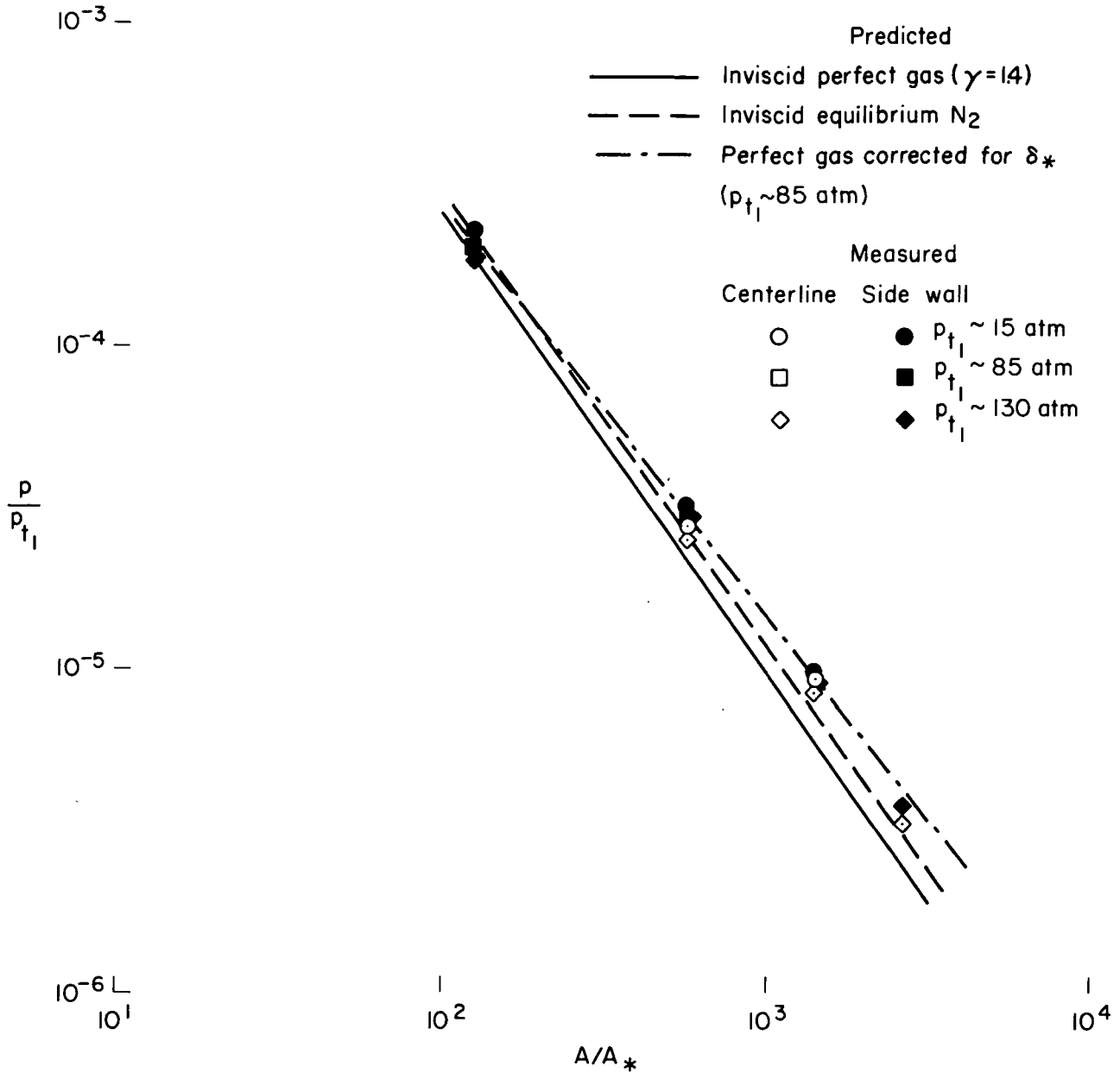

Figure 6.– Comparison of measured and predicted axial static-pressure distributions in nozzle for N_2.

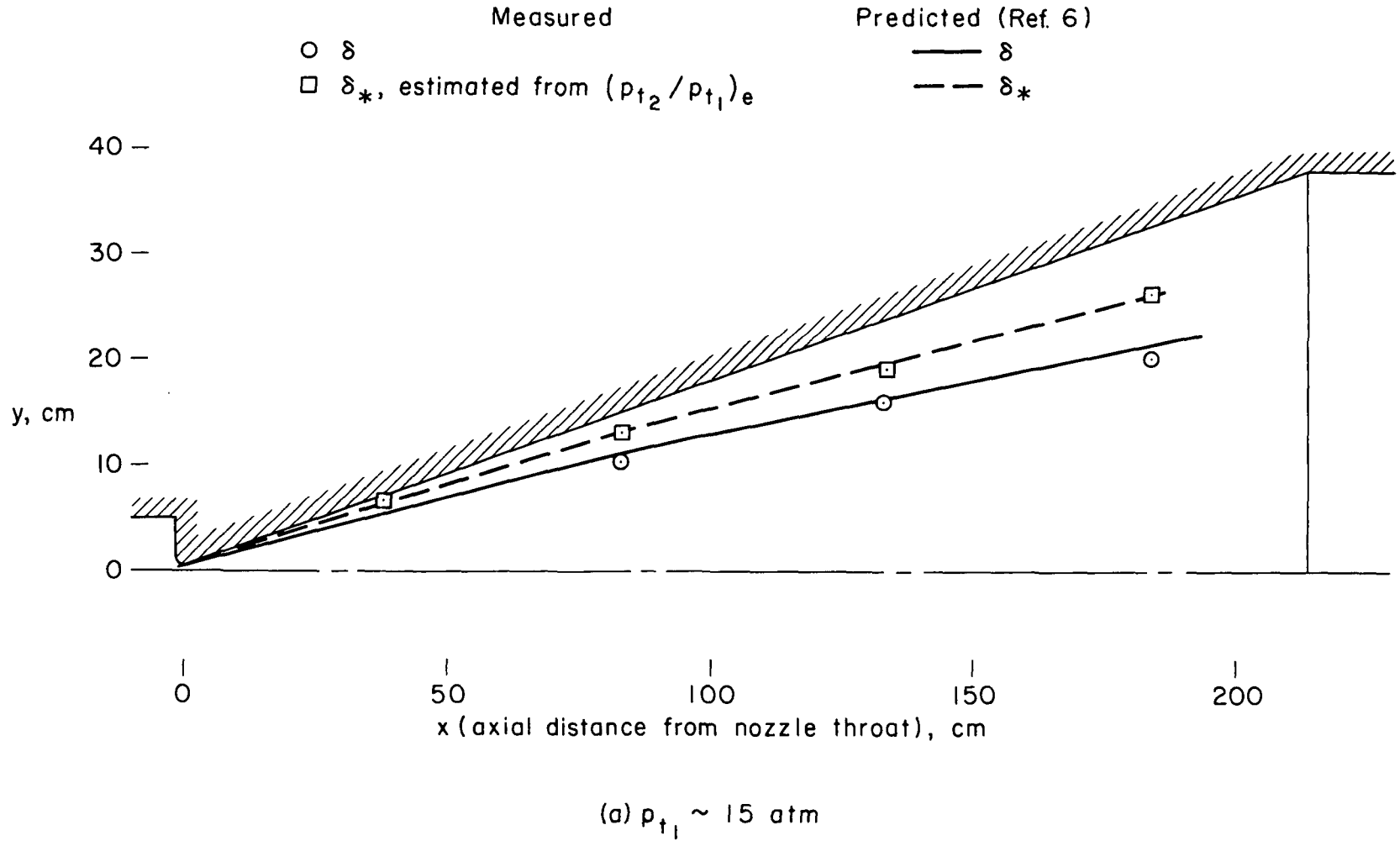

Figure 7.– Comparison of measured and predicted boundary-layer growth in nozzle for N_2.

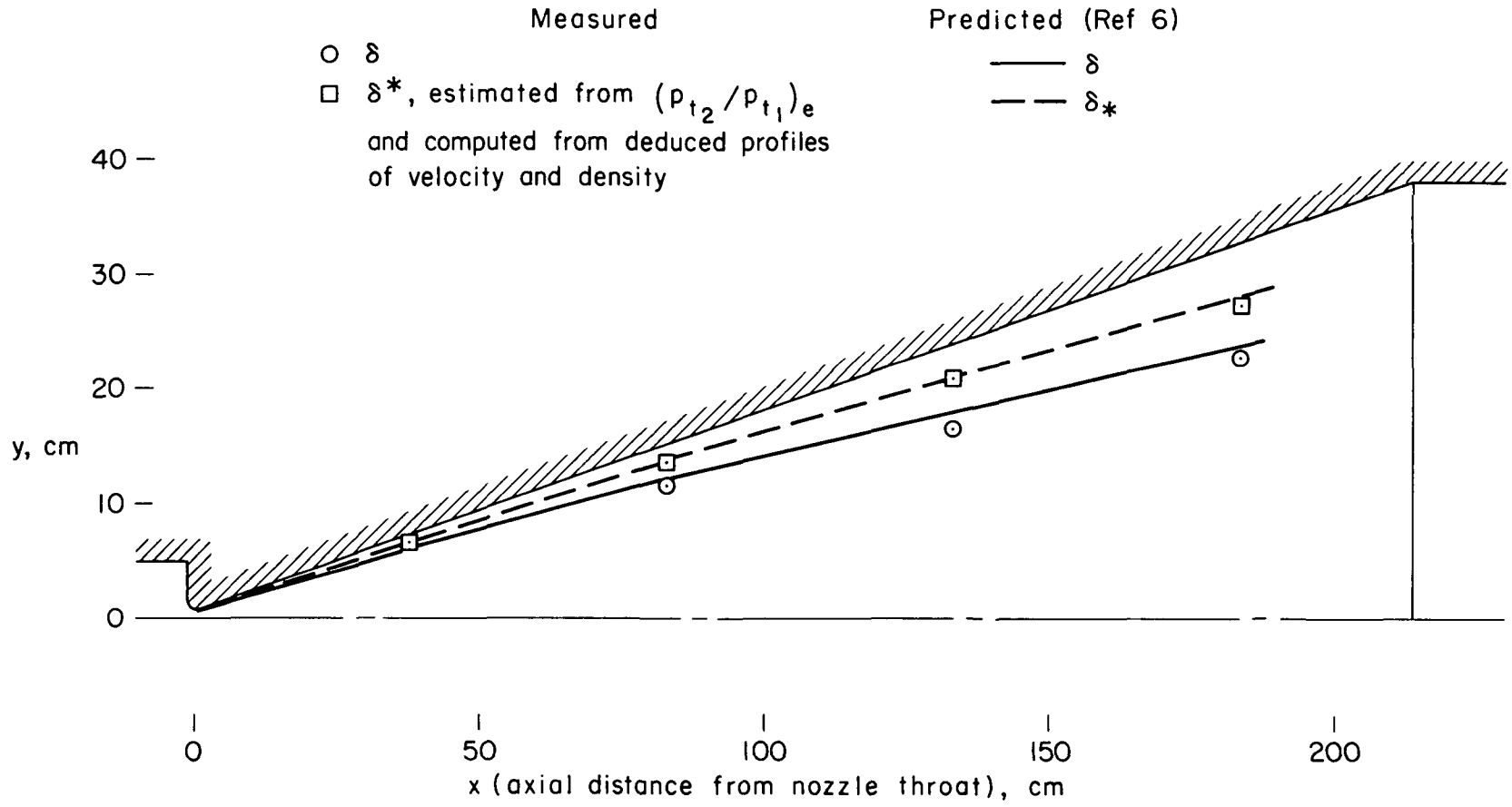

(b) $p_{t_1} \sim 85$ atm

Figure 7. – Continued.

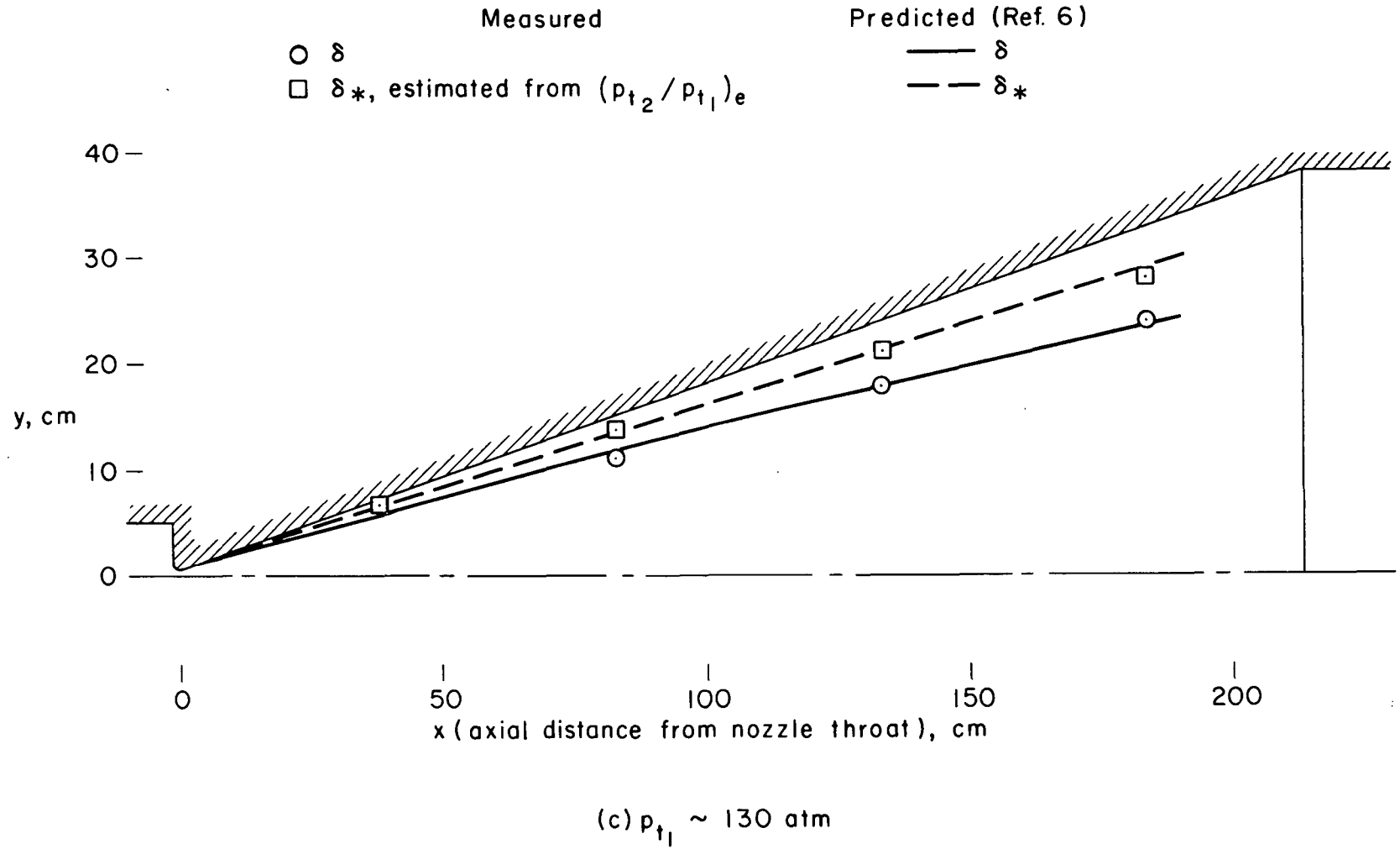

Figure 7.– Concluded.

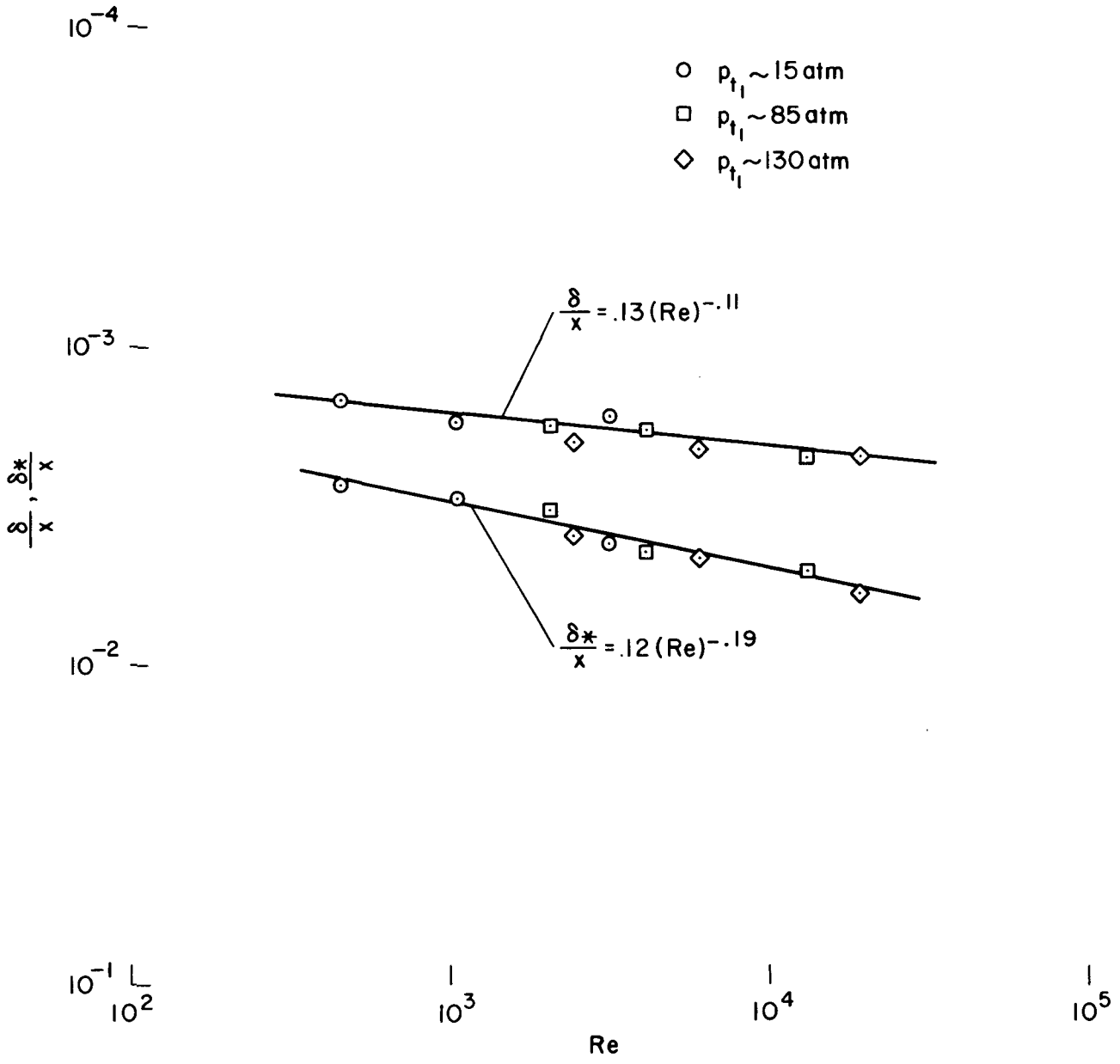

Figure 8.– Correlation of boundary-layer thickness and boundary-layer-displacement thickness for N_2.

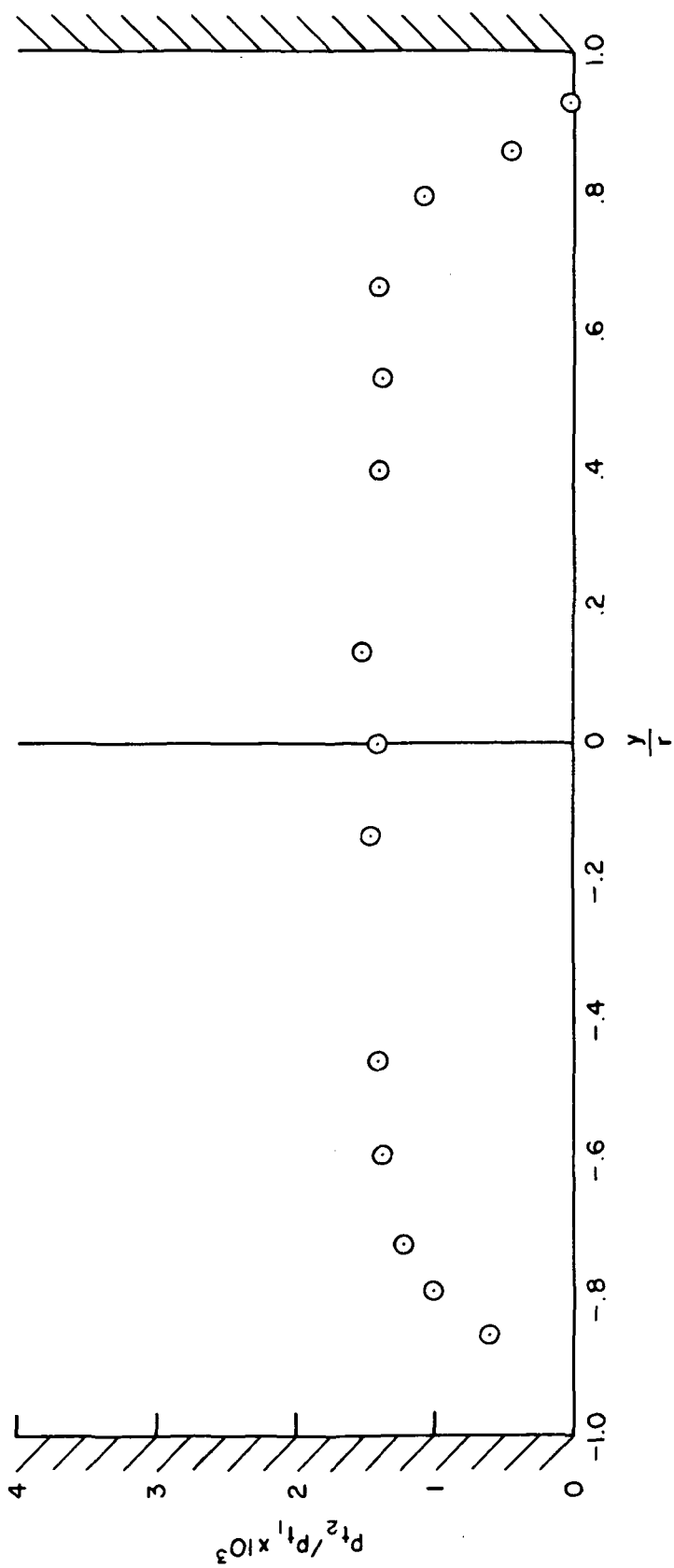

Figure 9.– Radial distribution of pitot pressure in Ar at $A/A_* = 1444$; p_{t_1} ~85 atm, T_t ~2000° K.

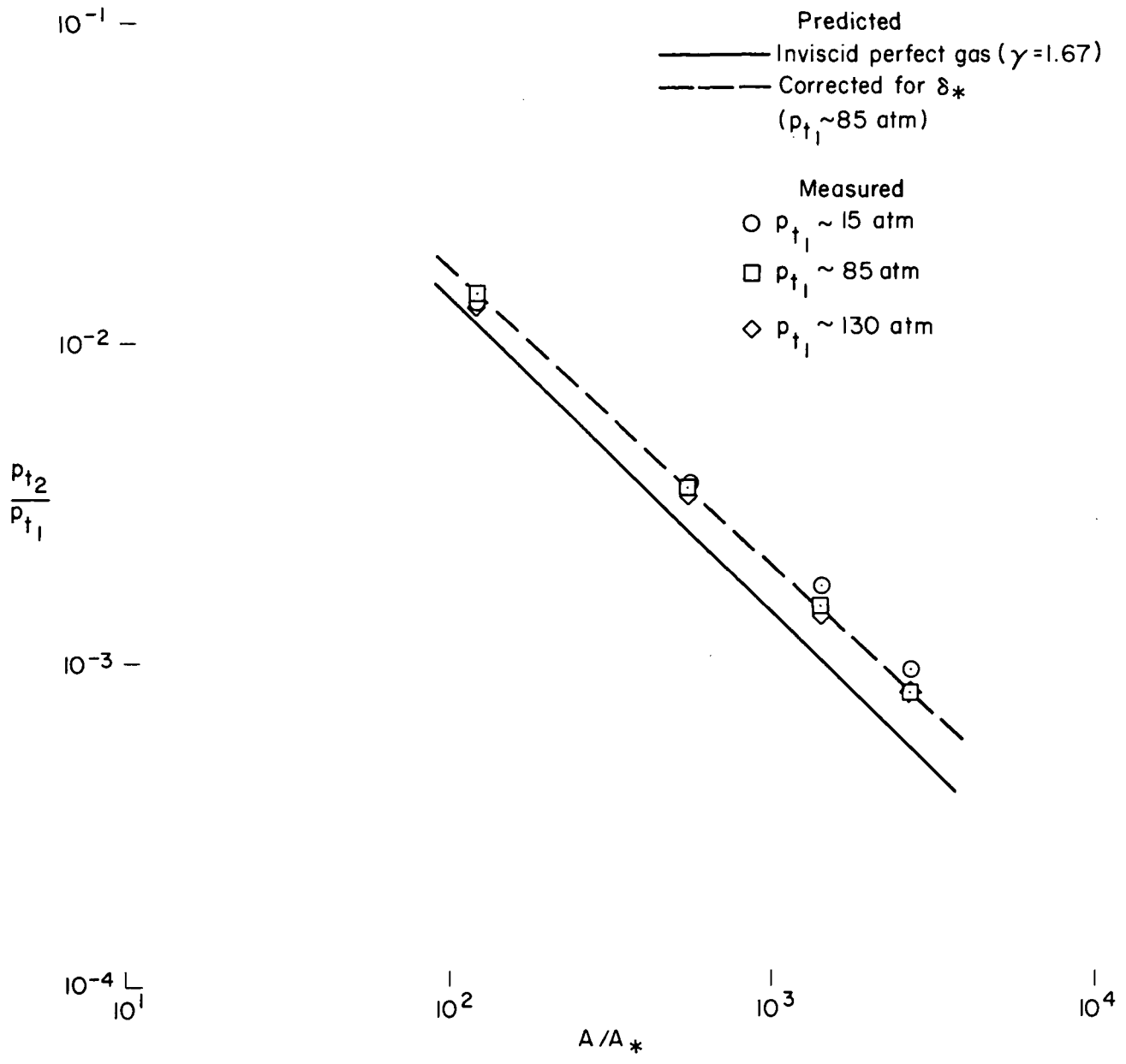

Figure 10. – Comparison of measured and predicted axial pitot-pressure distributions in nozzle for Ar.

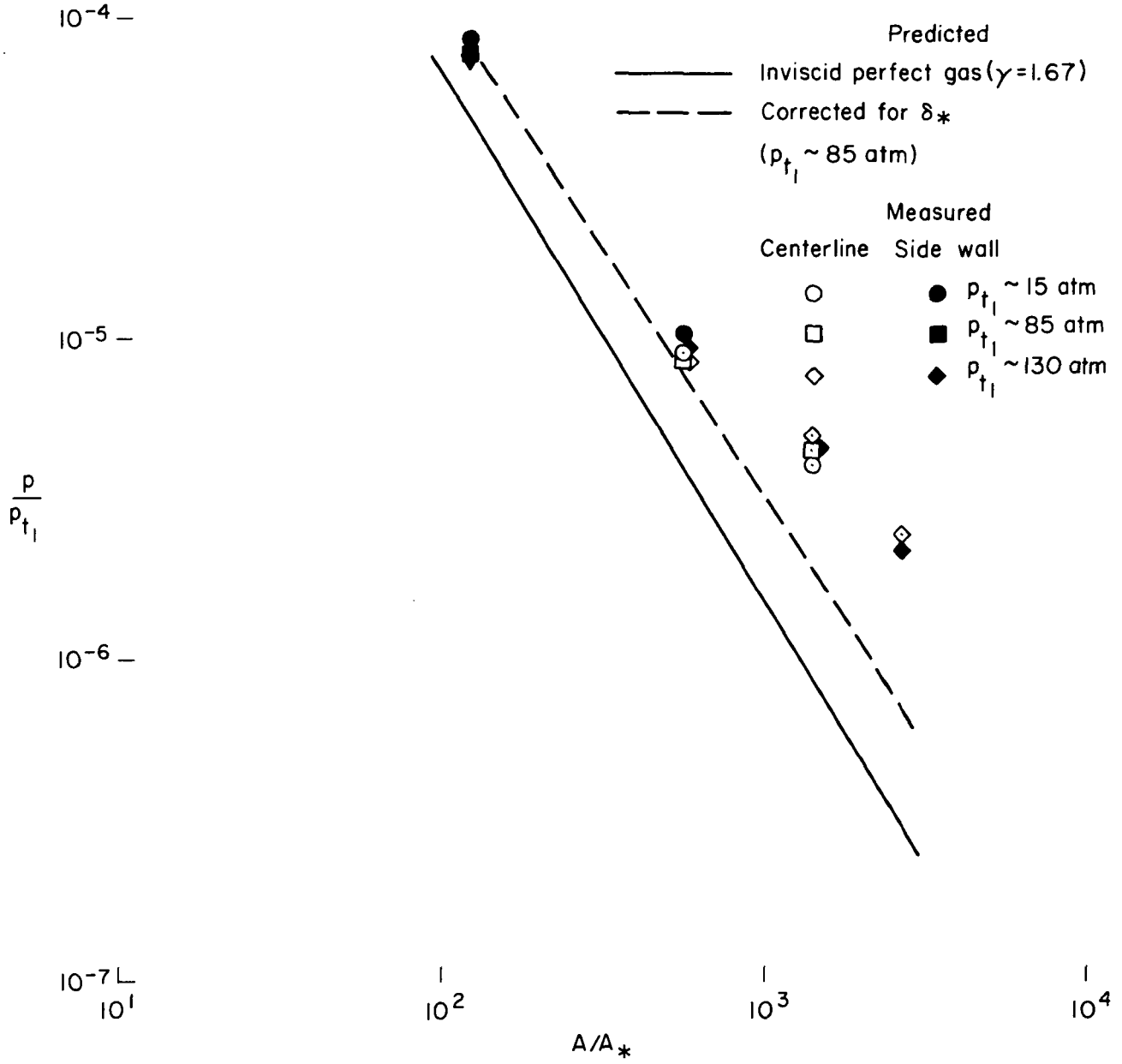

Figure 11.– Comparison of measured and predicted axial static-pressure distributions in nozzle for Ar.

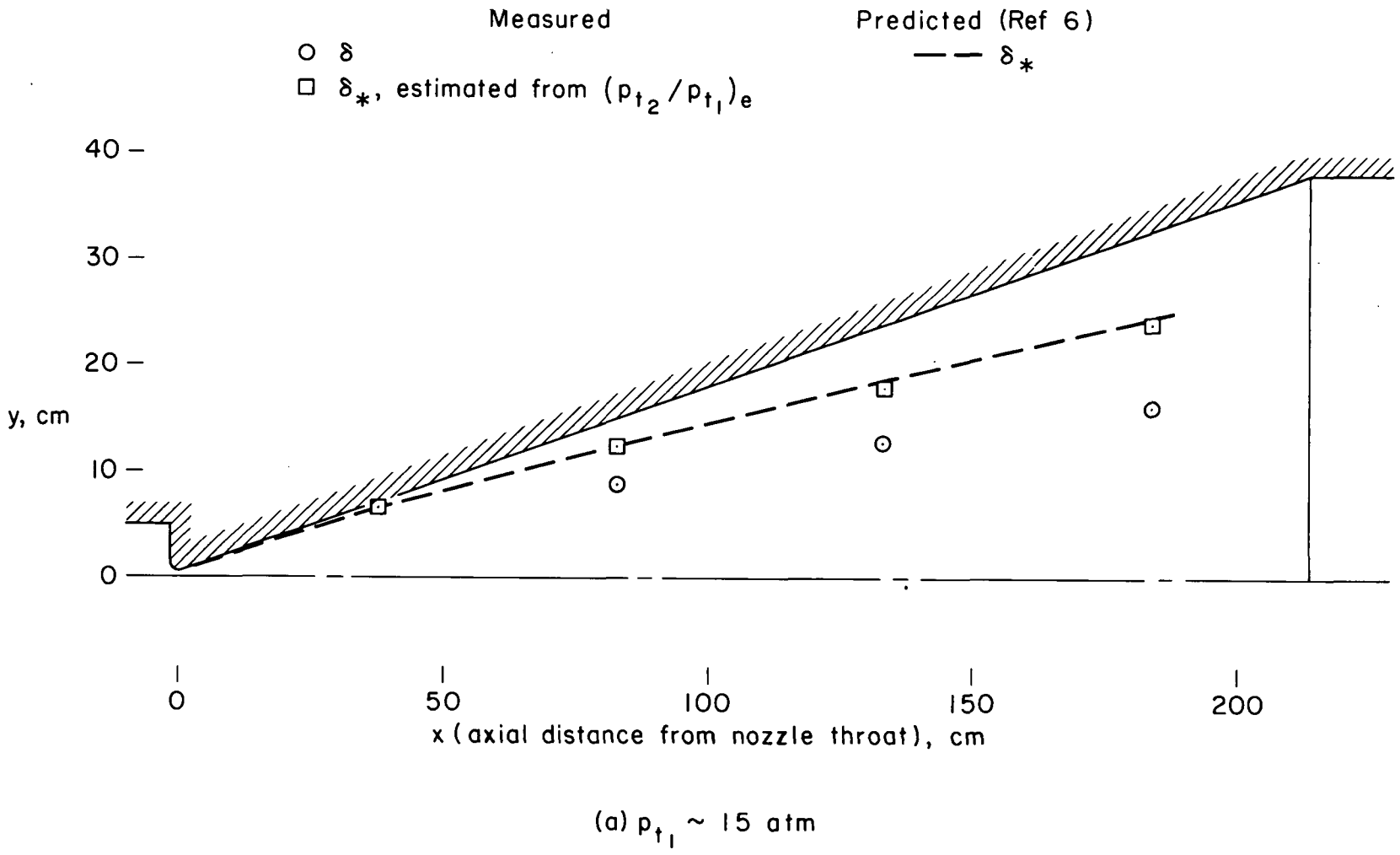

Figure 12.– Comparison of measured and predicted boundary-layer growth in nozzle for Ar.

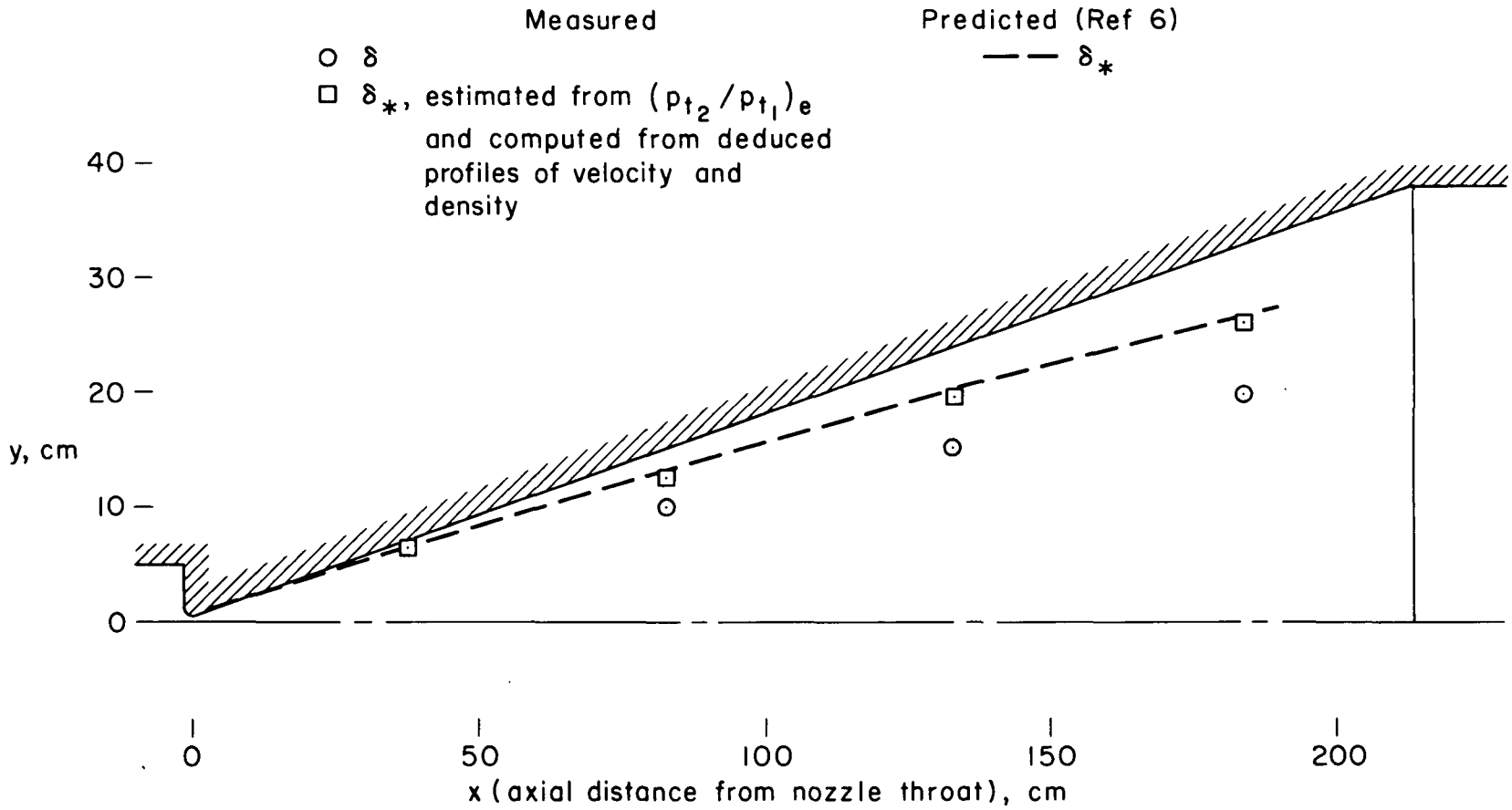

(b) $p_{t_1} \sim 85$ atm

Figure 12.– Continued.

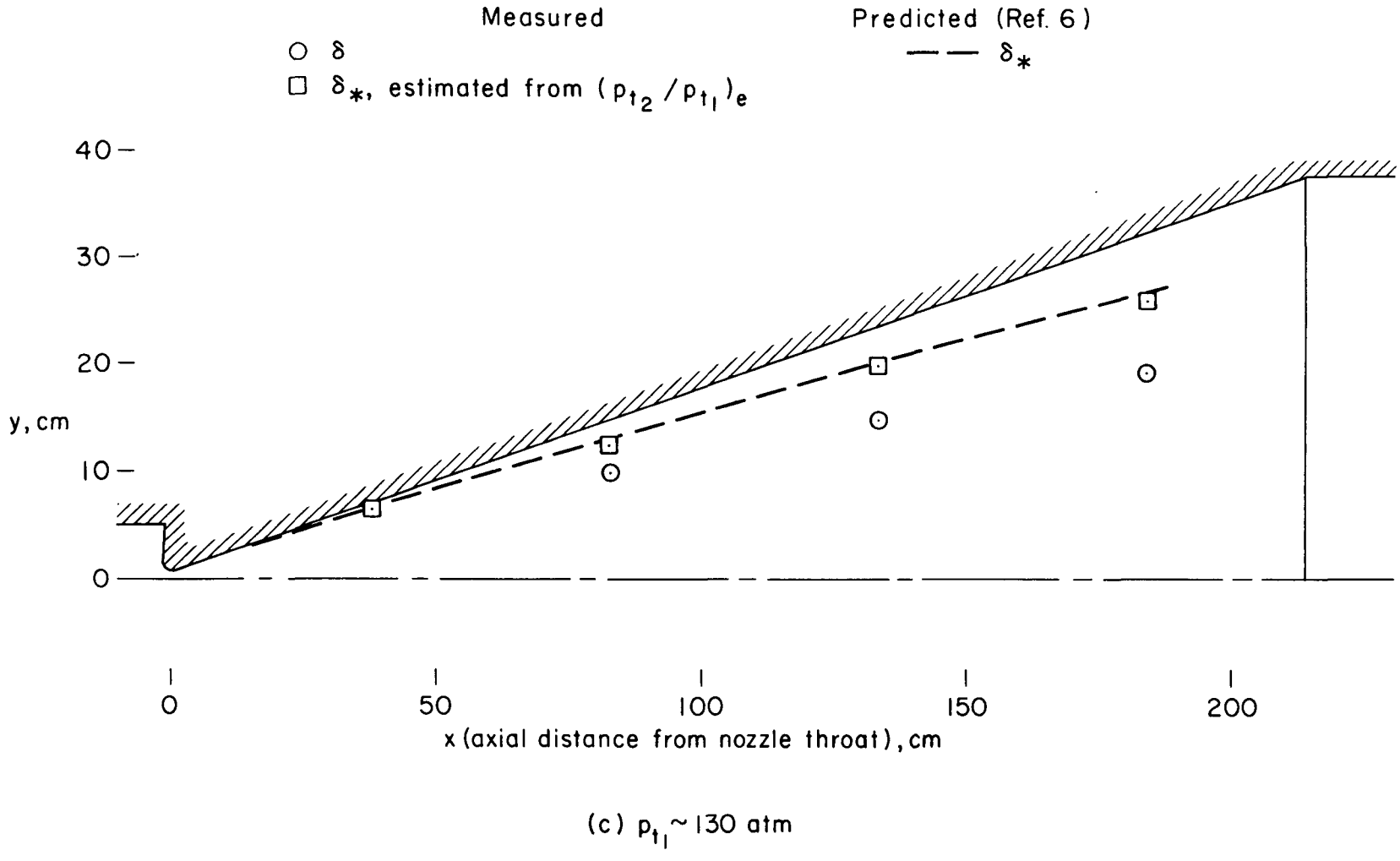

Figure 12.– Concluded.

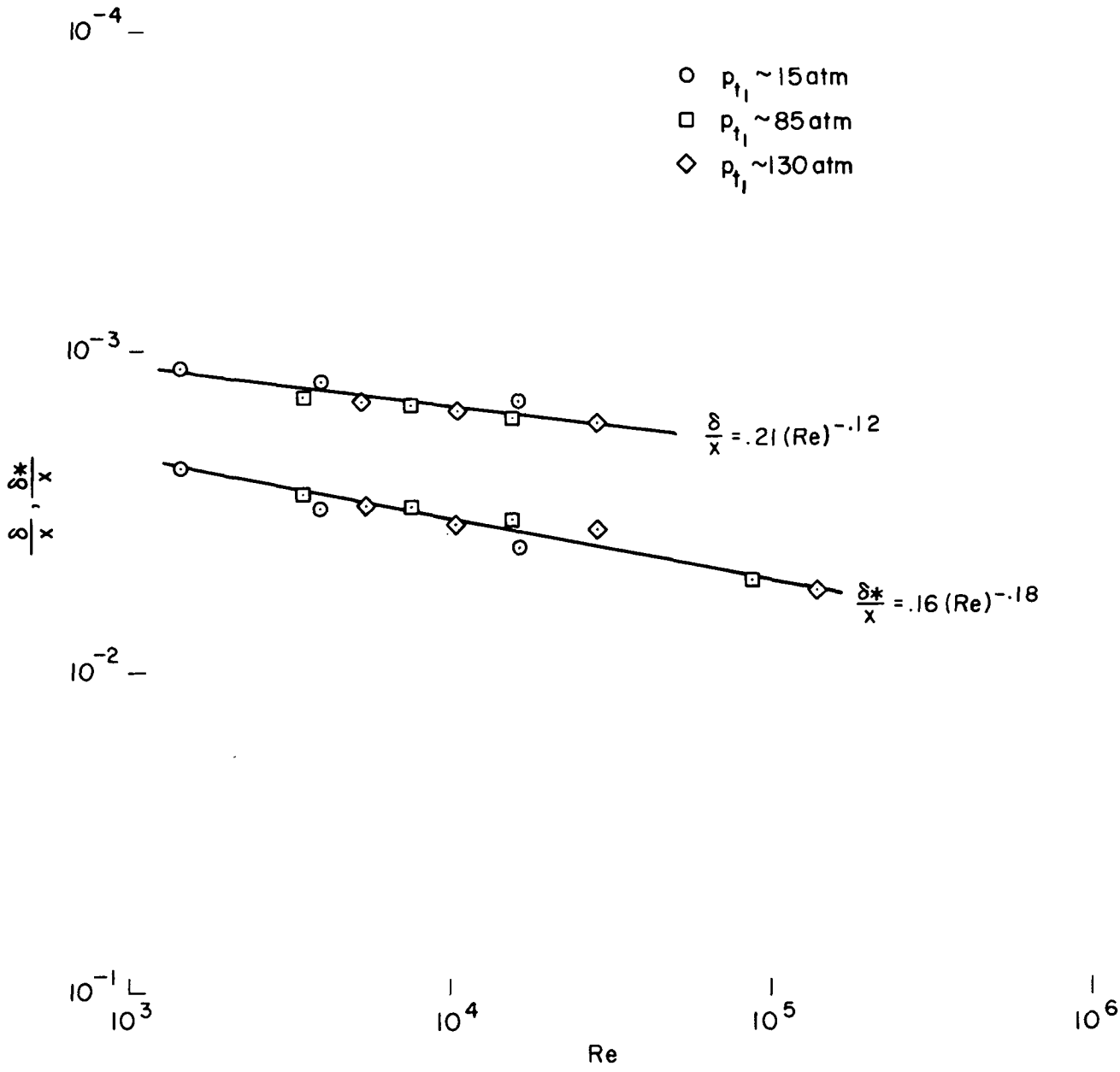

Figure 13.– Correlation of boundary-layer thickness and boundary-layer-displacement thickness for Ar.

ATIONAL AERONAUTICS AND SPACE ADMINISTRATION
WASHINGTON, D.C. 20546

OFFICIAL BUSINESS
PENALTY FOR PRIVATE USE $300

SPECIAL FOURTH-CLASS RATE
BOOK

POSTAGE AND FEES PAID
NATIONAL AERONAUTICS AND
SPACE ADMINISTRATION
451

U.S.MAIL

POSTMASTER : If Undeliverable (Section 158 Postal Manual) Do Not Return

"The aeronautical and space activities of the United States shall be conducted so as to contribute . . . to the expansion of human knowledge of phenomena in the atmosphere and space. The Administration shall provide for the widest practicable and appropriate dissemination of information concerning its activities and the results thereof."

—NATIONAL AERONAUTICS AND SPACE ACT OF 1958

NASA SCIENTIFIC AND TECHNICAL PUBLICATIONS

TECHNICAL REPORTS: Scientific and technical information considered important, complete, and a lasting contribution to existing knowledge.

TECHNICAL NOTES: Information less broad in scope but nevertheless of importance as a contribution to existing knowledge.

TECHNICAL MEMORANDUMS: Information receiving limited distribution because of preliminary data, security classification, or other reasons. Also includes conference proceedings with either limited or unlimited distribution.

CONTRACTOR REPORTS: Scientific and technical information generated under a NASA contract or grant and considered an important contribution to existing knowledge.

TECHNICAL TRANSLATIONS: Information published in a foreign language considered to merit NASA distribution in English.

SPECIAL PUBLICATIONS: Information derived from or of value to NASA activities. Publications include final reports of major projects, monographs, data compilations, handbooks, sourcebooks, and special bibliographies.

TECHNOLOGY UTILIZATION PUBLICATIONS: Information on technology used by NASA that may be of particular interest in commercial and other non-aerospace applications. Publications include Tech Briefs, Technology Utilization Reports and Technology Surveys.

Details on the availability of these publications may be obtained from:

SCIENTIFIC AND TECHNICAL INFORMATION OFFICE

NATIONAL AERONAUTICS AND SPACE ADMINISTRATION

Washington, D.C. 20546